

Preformed template fluctuations promote fibril formation: Insights from lattice and all-atom models

Maksim Kouza*

*Faculty of Chemistry University of Warsaw,
ul. Pasteura 1, 02-093 Warszawa Poland*

Nguyen Truong Co

*Saigon Institute for Computational Science and Technology, 6 Quarter,
Linh Trung Ward, Thu Duc District, Ho Chi Minh City, Vietnam*

Phuong Hoang Nguyen

*Laboratoire de Biochimie Theorique, UPR 9080 CNRS, IBPC,
Universite Paris 7, 13 rue Pierre et Marie Curie, 75005, Paris, France*

Andrzej Kolinski

*Faculty of Chemistry, University of Warsaw,
ul. Pasteura 1, 02-093 Warszawa Poland*

Mai Suan Li[†]

*Institute of Physics, Polish Academy of Sciences,
Al. Lotnikow 32/46, 02-668 Warsaw, Poland*

(Dated: February 27, 2015)

Fibril formation resulting from protein misfolding and aggregation is a hallmark of several neurodegenerative diseases such as Alzheimer's and Parkinson's diseases. Despite the fact that the fibril formation process is very slow and thus poses a significant challenge for theoretical and experimental studies, a number of alternative pictures of molecular mechanisms of amyloid fibril formation have been recently proposed. What seems to be common for the majority of the proposed models is that fibril elongation involves the formation of pre-nucleus seeds prior to the creation of a critical nucleus. Once the size of the pre-nucleus seed reaches the critical nucleus, its thermal fluctuations are expected to be small and the resulting nucleus provides

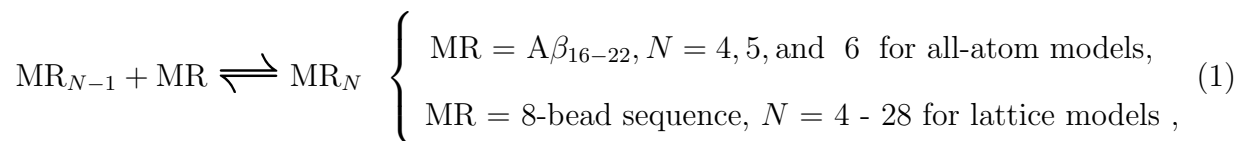
a template for sequential (one-by-one) accomodation of added monomers. The effect of template fluctuations on fibril formation rates has not been explored either experimentally or theoretically so far. In this paper we make the first attempt at solving this problem by two sets of simulations. To mimic small template fluctuations, in one set, monomers of the preformed template are kept fixed, while in the other set they are allowed to fluctuate. The kinetics of addition of a new peptide onto the template is explored using all-atom simulations with explicit water and the GRO-MOS96 43a1 force field and simple lattice models. Our result demonstrates that preformed template fluctuations can modulate protein aggregation rates and pathways. The association of a nascent monomer with the template obeys the kinetics partitioning mechanism where the intermediate state occurs in a fraction of routes to the protofibril. It was shown that template immobility greatly increases the time of incorporating a new peptide into the preformed template compared to the fluctuating template case. This observation has also been confirmed by simulation using lattice models and may be invoked to understand the role of template fluctuations in slowing down fibril elongation *in vivo*.

I. INTRODUCTION

Alzheimer's, Parkinson's, Huntington's, type II diabetes, mad cow disease and cystic fibrosis: these apparently unrelated diseases, the so-called protein structural diseases, are found to be a result of protein misfolding¹. This has spurred many experimental¹⁻¹¹ and theoretical studies¹²⁻²⁷ to understand factors and mechanisms that drive oligomer formation. Aggregation rates depend not only on protein sequence, but also on the concentration of proteins and external conditions like temperature, pH, presence of crowding agents, etc. The observation that many proteins that are unrelated by sequence and structure can aggregate and form fibrils¹ with similar morphologies suggests certain generic aspects of oligomerization.

There are a number of mechanisms for fibril elongation such as the so called templated-assembly mechanism²⁸⁻³¹, nucleation-growth³² and nucleated conformational conversion^{2,33}). Experimental^{28,34} and theoretical^{23,30,35} studies suggest that in the templated-assembly scenario the association of monomers to the preformed fibril follows the dock-lock mechanism, i.e. a nascent monomer can dock and then undergo the needed structural arrangement to lock onto the template. In the previous work³⁰ it has been suggested that a template of a few peptides fluctuates a lot to accommodate a nascent monomer. However, the question as to what extent the fluctuation modulates the fibril formation rate remains open. In the present paper we consider this problem assuming that the growth of fibrils occurs by addition of one unstructured monomer at a time³⁴ and that fluctuations of the preformed template are small provided its number of monomers exceeds the size of critical nucleus N_c .

Because in simulations we can only deal with a limited number of monomers to mimic weak fluctuations of the template we kept C_α positions of the template fixed during simulations. Such a template will be referred to as the fixed template (FT). To study the effect of fluctuations on fibril formation rates, we considered the non-fixed template (NFT) in which monomers of the preformed template are allowed to move. Initial configurations of FT and NFT were chosen to be the same. The kinetics of association of an added monomer with the preformed FT and NFT is monitored by studying the following reaction (Eq. 1):



where MR stands for the monomer. Because simulations of fibril formation by long peptides and proteins are very CPU consuming, for all-atom models we chose the Gromos96 43a1 force field³⁶ and short amyloid peptide $A\beta_{16-22}$ ³⁰. In the lattice model, MR is an 8-bead monomer³⁷. **To assure the robustness of main results against template structures we have also performed limited all-atom simulations for (8+1)-systems of fragment $A\beta_{16-21}$ for which the double-layered protofibril structure was experimentally resolved.**

Our study of reaction (1) with FT and NFT shows that the immobility of templates greatly slows down the fibril elongation process. This main result, based on both all-atom and coarse-grained lattice models, may be invoked to understand why fibril growth above the critical nucleus with small fluctuations of the preformed template is still very slow.

Overall, we present evidence that in the case of FT the fibril state might be reached along alternative slow kinetics pathways. Since the fixation of backbone atoms makes the template more rigid, it mimics the decreased backbone entropy. An intriguing conclusion one might propose that fast kinetics in case of NFT is entropy-driven, e.g. an increase in backbone entropy facilitates the kinetics of fibril formation.

II. METHODS/EXPERIMENTAL SECTION

A. All-atom models

We used the GROMOS96 43a1 force field³⁶ to model $A\beta_{16-22}$ peptides, and SPC water model³⁸ to describe the solvent. This model has been successfully used for studying protein folding³⁹, unfolding⁴⁰ and aggregation^{41,42}. The simulations were performed for systems with FT, while the corresponding systems with NFT have been studied in our earlier work³⁰. Gromacs version 4 was employed for the simulations.

1. Templates and an added peptide.

The initial conformation for the nascent peptide $A\beta_{16-22}$ used in the simulations was extracted from the structure of the $A\beta_{10-35}$ peptide available in the Protein Data Bank (ID: 1hz3)⁴³. The terminal residues are oppositely charged (a positive charge on the lysine and a negative charge on the glutamic acid). For the templates we used antiparallel configurations of $A\beta_{16-22}$ peptides obtained by long molecular dynamics (MD) all-atom simulations in our

previous work³⁰. The templates for the three systems studied in this paper are shown in Fig. 1. **During all-atom FT simulations we kept C_α positions of the template frozen to prevent template disassembly. All others atoms of template were allowed to move without any restraints.** The added monomer is randomly put next to the template and the same starting conformations for both FT and NFT are used.

2. Details of MD runs.

For each system we performed 8 MD runs (trajectories), the durations of which are given in Table 1. The typical volumes of boxes used in the simulations are 62, 86, and 130 nm³ for (3+1), (4+1) and (5+1) systems, respectively. This corresponds to peptide concentrations of 112, 99, and 80 mM which are about two orders of magnitude as high as those used in the experiments¹.

3. Principal component analysis.

We used dihedral principal component analysis (dPCA)⁴⁴ to represent the free energy landscape (FEL) of the $3N$ -dimensional system. Free energy is calculated as a function of the first two eigenvectors V_1 and V_2 in dPCA. **Note that FEL is not equilibrium FEL but rather to present probabilities of different structures to occur during MD simulations.**

4. Measures used in structure analysis.

To characterize the fibril state of short peptides we used not only nematic order parameter P_2 ^{30,45}, but also took into account the number of backbone hydrogen bonds (HBs) between nascent peptide and FT. This more strict condition prevents false signals of an ordered state including cases where nascent peptide has high P_2 but is located either far from the template or above/below the template. If P_2 is larger than 0.8 and the number of average backbone HBs is larger than 3 then the system is considered to be in an ordered state. A visual inspection was also performed to exclude the configurations with a parallel arrangement of β -strands. The time to incorporate a nascent peptide to the template, τ_{inc} is defined as the first passage time to reach an antiparallel ordered structure starting from a preformed

template and a randomly added peptide. The median time serves as an estimate of the oligomerization time for each of studied systems. As we have 8 trajectories for each system, the median is defined as the mean of the 4th and 5th values.

B. Lattice model

To overcome the limits set by expensive all-atom modeling, coarse-grained lattice models might be successfully utilized for protein folding studies⁴⁶⁻⁴⁸. In this work we use the toy lattice model which has been developed for studying oligomerization kinetics³⁷. Typically, each chain consists of M connected beads confined to the vertices of a cube. The simulations use N identical chains and $M = 8$. The sequence of a chain is +HHPPHH-, where + and - are charged beads. H and P refer to hydrophobic and polar beads, respectively. Despite the simplicity of the lattice model, it has been proved to be useful in providing insights into fibril formation mechanisms.

The inter- and intra-chain potentials include excluded volume and nearest-neighbor contact interactions. Excluded volume is imposed by the condition that a lattice site can be occupied by only one bead. The energy of n chains is

$$E = \sum_{l=1}^N \sum_{i<j}^M e_{sl(i)sl(j)} \delta(r_{ij} - a) + \sum_{m<l}^N \sum_{i,j}^M e_{sl(i)sm(j)} \delta(r_{ij} - a), \quad (2)$$

where r_{ij} is the distance between residues i and j , a is lattice spacing, $sm(i)$ indicates the type of residue i from the m -th peptide, and $\delta(0) = 1$ and zero, otherwise. The first and second terms in Eq. 2 represent intrapeptide and interpeptide interactions, respectively.

Contact energy between H beads e_{HH} is -1 (in hydrogen bond energy units ϵ_H). The propensity of polar (including charged) residues to be "solvated" is mimicked using $e_{P\alpha} = -0.2$, where $\alpha = P, +, \text{ or } -$. "Salt-bridge" formation between oppositely charged beads is accounted for by a favorable contact energy $e_{+-} = -1.4$. All other contact interactions are repulsive. The generic value for repulsion $e_{\alpha\beta} = 0.2$. For a pair of like-charged beads the repulsion is stronger, i.e. $e_{++} = e_{--} = 0.7$. The chains are confined to the vertices of the three-dimensional hypercube. Monomer concentration is kept at ≈ 6 mM (the cubic size is roughly $35a$ for $N = 10$ monomers) for all systems. This is roughly one order of magnitude denser than that used in typical experiments.

Simulations were performed by enclosing N chains in a box with periodic boundary conditions. We used the Monte Carlo (MC) **method** to study the kinetics of fibril formation. MC moves include global and local ones. A local move^{49,50} corresponds to tail rotation, corner flip, and crankshaft rotation. Global moves correspond to either translation of a peptide by a in a randomly chosen direction or rotation by 90° around one of the randomly chosen coordinate axes. Acceptance probabilities of global and local moves are 0.1 and 0.9, respectively (see Ref.³⁷ for more details). We measure time in units of Monte Carlo steps (MCS). The combination of local and global moves constitutes one MCS. **Although the correspondence between real time and MC step is not clear, as shown previously, our MC method is still useful to compare kinetics of different systems**^{26,37,51,52}.

Initial conformations have a preformed template with N antiparallel chains and one chain which is randomly added next to the template (see below). As in the all-atom model case, τ_{inc} is defined as the number of MCS's needed to reach the mature N -chain fibril which has the lowest energy. The fibril state is characterized by the number of inter-chain contacts which are called fibril contacts.

III. RESULTS AND DISCUSSION

A. All-atom model

1. Diversity of fibril formation kinetics: Peptide association may proceed via intermediates.

As shown by experiments and simulations^{30,31,34}, the addition of a new monomer onto a growing template obeys the two-stage dock-lock mechanism. It is worth noting that amyloid fibrils are characterized not only by ordered peptides perpendicular to the fibril axis, but also by backbone HBs between them parallel to the fibril axis. For a mobile template the kinetics is simple³⁰. First, a nascent peptide rapidly docks to the edge of the preformed template, then it reaches the fibril state through a slower locking stage. The conformations with high beta content and P_2 values are identified as fibril-like conformations where a nascent peptide is tied to the preformed template by backbone HBs. Although such correspondence between high P_2 values and a large number of HBs works for NFT, it becomes insufficient for FT. In this case there exist a number of trajectories where the ordered peptide (with P_2 values > 0.8) has no more than 1 backbone hydrogen bond with the template (Tr4 and Tr5 in Fig.

2, Tr4, Tr5 and Tr6 in Fig. 3, and Tr1, Tr3, Tr5 and Tr7 in Fig. 4). In such trajectories a nascent peptide is directed into the position above the template in which it predominantly interacts with a template through SC-SC interactions. In other words, although the nascent peptide is extended and oriented in the right direction, backbone HBs with the template are not formed and those conformations do not correspond to the fibril state. Thus, we use the number of backbone HBs between a nascent monomer and a template as an additional (unambiguous) indicator of the fibril state. The simple definition involving $P_2 > 0.8$ and more than three backbone HBs between the monomer and the template, defines the fibril state in a well-defined manner.

As evident from Figs. 2-4 there are fast and slow kinetics routes toward the fibril state. We interpret the slow kinetics pathways as a sign of the occurrence of the intermediate state which corresponds to a plateau on the curve of time dependence of the order parameter P_2 . For (3+1) systems intermediates occur in Tr3, Tr4, Tr5 and Tr6 (Fig. 2), while the fibril state was reached in other MD runs at relatively short time scales. In (4+1) systems intermediate states were observed in Tr1, Tr5 and Tr6 where the ordered state did not appear during the whole simulation course (Fig. 3). Particularly, two intermediates with $P_2 \approx 0.1$ and 0.65 occurred in Tr6. We also see short-lived intermediates in Tr2, Tr3 and Tr8. For (5+1) systems there is clear evidence for the existence of intermediates in Tr3, Tr4, Tr5, Tr6, Tr7 and Tr8 where the fibril-like state did not appear during the whole MD run (Fig. 4). In Tr7 there are at least two intermediates. The anti-parallel configuration is reached relatively rapidly in the remaining trajectories.

We observe a parallel orientation of peptides (Fig.3, Tr1 and 4, Tr2) which is one of the obstacles that complicate aggregation kinetics. In the case of 4+1 system (Fig. 3, Tr1), we do not observe transition from a parallel to antiparallel configuration for 500 ns, while for 5+1 system (Fig. 4, Tr2) it takes about three hundred nanoseconds for the fibril state to occur. For the 4+1 system the parallel orientation detected in our FT simulation is a sign of the intermediate state. However, because the average addition time for 5+1 system exceeds 220 ns, it is not clear whether such a conformation is on a pathway to intermediates but transitions from parallel to antiparallel configurations are apparently expected to slow aggregation.

2. *Association of a new monomer with the fixed template depends on initial conditions.*

It is evident from Fig. 2–4 that τ_{inc} greatly varies from trajectory to trajectory. One of the reasons for this is that we used different starting configurations for a nascent monomer for different runs keeping the same FT for all 8 trajectories. For trajectory 8 of the (3+1)-system, in which the fibril structure is formed, the added monomer is initially located aside the template (Fig. 5, Tr8). This initial configuration is strikingly different from that of the slowest trajectory 3 (Fig. 5, Tr3). Here the nascent monomer is located above (or below) the template and nearly perpendicular to the preformed chains. The difference in starting configurations leads to different FELs (Fig. 5). Typical free energy barriers separating main basins of the fast trajectory 8 are about 5 kJ/mol compared to ≈ 14 kJ/mol for the slow trajectory 3. In the former case the high mobility of a nascent monomer caused by the flat FEL facilitates fibril formation. For trajectory 3, due to high free energy barriers the system may get trapped in local minima that hinder the formation of ordered fibrils. The difference in free energy barriers, $\Delta\Delta G \approx 14 - 5 = 9$ kJ/mol leads to the difference in aggregation rates of about two orders of magnitude at room temperature.

The dependence of FEL on initial configurations is also illustrated in Fig. 5 for two trajectories 2 and 3 of the (5+1)-system. Similarly to the (3+1) case, if the added monomer is initially positioned aside the template, FEL is more flat (trajectory 2) than when the nascent peptide is positioned above/below the template (trajectory 3). In the latter case FEL consists of isolated pieces leading to slow fibril elongation. As follows from Fig. 5c and 5d the difference in free energy barriers between main basins is also about 10 kcal/mol.

3. *Immobility of the template slows down the fibril formation process.*

(3+1)-system. In contrast with NFT simulations³⁰, our results indicate that kinetics is much more complex and diverse for FT. The fibril state occurs very fast with $\tau_{\text{inc}} \approx 19.4$, 43.5 and 13.5 ns for Trajectory 1, 7 and 8, respectively. The fibril state is not stable for Trajectory 1 and 7, because peak P_2 drops at ≈ 92 and ≈ 50 ns, respectively, and fluctuates around a moderate value. (Fig. 2, Tr1 and Tr7). Such instability is due to shallow free energy barriers (Fig. 5, Tr1) and a nascent peptide can easily jump from one basin to another. As a result, after about 100 ns the fibril state reoccurs in Tr7, but not in Tr1. The

eighth trajectory represents an example of a fast aggregation pathway at which the fibril state remains stable. Remarkably, the fibril structure does not appear in MD runs 3 and 4. For the third run the order parameter P_2 and average number of HBs remain low for 500 ns. Much higher P_2 values are observed for trajectory 4, but the low number of backbone HBs does not guarantee the occurrence of the fibril state (Fig. 2, Tr4). Typical snapshots shown in Fig. 2, Tr3 and Tr4 indicate that in cases where fibril structure is not formed or formed very slowly (Fig. 2 Tr2 and Tr5), the nascent peptide is directed into a state above the template in which it predominantly interacts with the template through SC-SC interactions. We have interpreted such slow kinetics pathways as a sign of an intermediate state, where the slow phase is associated with crossing over the high barrier from off-pathway intermediate states to the fibril-like ones. This can be also interpreted as getting out of conformations above/below the template to the edge of the template before the docking phase begins.

Calculating the median time over eight trajectories, we obtain $\bar{\tau}_{inc} \approx 242.9$ ns for the (3+1)-system. This value is much larger than $\bar{\tau}_{inc} \approx 23$ ns obtained for the case where the template is not fixed³⁰ (Table 1). Thus template immobility considerably slows down the association of a nascent peptide with the preformed oligomer.

(4+1)-system.

The nascent peptide and preformed template form a fibril in trajectories 2-4, 7 and 8, where τ_{inc} varies from ≈ 31.5 to ≈ 486 ns (Fig. 3). For the first MD run the fibril-like state is observed but with a parallel orientation. Thus τ_{inc} for the expected antiparallel ordering should be longer than the whole run of 500 ns. This is supported by the snapshot collected when P_2 reaches one of the highest values. P_2 becomes relatively high after 100 and 282 ns for trajectories 5 and 6. However, a fibril is not formed due to a very low value of backbone HBs between the added peptide and FT. Using the results shown in Table I we obtain median time $\bar{\tau}_{inc} \approx 456.5$ ns which is larger than $\bar{\tau}_{inc} = 114$ ns for NFT³⁰ (Table II).

Interestingly, the off-pathway intermediate and parallel configurations typical for slow pathways were not observed in NFT simulations³⁰. Thus, the reduced flexibility of a template with a lower level of complexity allows a nascent peptide to visit a larger number of conformation states compared to NFT. This includes both off-pathway intermediate and parallel ordered conformations, which requires an extra barrier to be overcome for fibrils to occur.

(5+1)-system. The slowing down of the peptide association process by template immo-

bility is also seen in the (5+1)-case (Fig. 4). An antiparallel fibril occurs at $\tau_{\text{inc}} \approx 179.5$, ≈ 321 and ≈ 212 ns for the first, second and fourth trajectory, respectively. For trajectories 3,5 and 6-8, at high P_2 values the nascent peptide gets trapped in a conformation and it is typically located above (or below) the template without a significant number of backbone HBs formed with FT. The fibril state does not appear after 500 ns (Table I). The median time calculated from 8 trajectories exceeds the duration of MD runs, $\bar{\tau}_{\text{inc}} > 500$ ns. Since for the NFT case the corresponding $\bar{\tau}_{\text{inc}} > 220$ ns³⁰ (Table II) our result suggests that template fixation slows down the association of a peptide to the preformed template but this conclusion is not as transparent as in (3+1) and (4+1) systems. Therefore, to clarify this point an additional simulation will be carried out using simple lattice models.

4. Robustness of results against data sampling

So far we have performed 8 independent MD runs for each system. The important question emerges is if this sampling is sufficient enough to not bias our main conclusions on the impact of template mobility on the kinetics behavior of the system. Because the all-atom simulation in explicit water is very time consuming we have carried 8 additional 500 ns runs for (4+1)-systems (Fig. S1 in the supplementary material⁵⁸ and Table I). Calculating the median time over 16 trajectories, we obtain $\bar{\tau}_{\text{inc}} \approx 492.5$ ns. This value is comparable to the median time $\bar{\tau}_{\text{inc}} \approx 456.5$ ns obtained for the first 8 trajectories of (4+1) system and which is larger than $\bar{\tau}_{\text{inc}} = 114$ ns for NFT. Thus the reduction of aggregation rates due to template immobility is robust against data sampling and this is expected to hold not only for the (4+1) system but also for other systems.

The diversity in kinetics routes to the fibril-like state is also observed in 8 additional trajectories (Fig. S1 in the supplementary material⁵⁸). For Tr9 the antiparallel arrangement occurred without intermediates but it is not the case for Tr11, Tr12 and Tr14 although their $\bar{\tau}_{\text{inc}}$ is shorter than the whole simulation time. A long-lived intermediate was observed in Tr11 where the parallel configuration appears at about 90 ns. The ordered state did not appear during the 500 ns MD simulation in Tr10, Tr13, Tr15 and Tr16. Taken together, the overall picture about complex kinetics pathways remains the same as in the case of 8 trajectories suggesting that the reduced entropy plays a decisive role but not the number of sampling.

5. Robustness of results against double-layered structure

Strickly speaking, the single layer structure of short peptides is neither amyloid fibril nor protofibril. To mimic protofibril in a more realistic way we consider a double-layered structure as template. Because the double-layered structure of $A\beta_{16-22}$ is not available we used the atomistic model proposed by the Eisenberg group⁵³ for $A\beta_{16-21}$ (KLVFFA). KLVFFA octamer (Fig. S2 in the supplementary material⁵⁸), extracted from KLVFFA dodecamer structure (pdb code: 3OW9), was chosen as a template. As in the single-layered case, the added monomer was randomly put next to the template so that no intermolecular contacts presented and the same starting conformations for both FT and NFT cases were used. The combined (8+1)-system were placed in a dodecahedron box of such a size that the minimal distance from peptides and the box is 1.75 nm. This was followed by solvation with 7734-9565 water molecules and nine chloride ions were added to neutralize the system charge. To avoid improper structures, the whole system was minimized with the steepest-descent method, before being equilibrated at 300K with two successive molecular dynamics runs of length 500 ps each; the first one at constant volume, the second at constant pressure (1atm). The equilibrated conformations were used as the starting structures for 200 and 400 ns MD simulations for NFT and FT, respectively. The simulations were performed at $T = 300$ K with the same force field and water model as in the single-layered structure case.

Out of 4 trajectories the antiparallel conformation was observed only in Tr4 for the FT case (Fig. S3 and Table S1 in the supplementary material⁵⁸). In contrast, for NFT the protofibril occured in all MD runs after relatively short times. We obtained $\bar{\tau}_{inc} \approx 84.35$ and > 500 ns for NFT and FT double layer systems, respectively. Thus, regardless of sequence and protofibril structure, the template immobility reduces the aggregation rate and this effect is universal and holds for other systems.

B. Lattice model

In this section we consider the kinetics of association of a new monomer to the preformed template using the lattice model³⁷. The reason for doing this is that, as follows from Table II, it remains uncertain within the all-atom model whether template immobility slows down the oligomerization of the (5+1)-system and this is also unclear for larger systems. Therefore,

our aim is to show that the irreversibility of aggregates affects the growth rate for large-size systems using the lattice model (2). The simplicity of this model allows us to study much larger systems compared to all-atom models.

1. *Template fixation increases τ_{inc} by one order of magnitude.*

The temperature dependence of τ_{inc} for the (5+1)-system with FT and NFT is shown in Fig. 6. As in the protein folding problem^{54,55}, the U-shape comes from the interplay between energy and entropy factors. At low T (energy driven regime), as T lowers the probability of escaping local minima decreases due to reduced thermal energy, resulting in higher τ_{inc} . At high T , where entropy dominates over energy, the thermal fluctuations are so high that the motion of chains becomes chaotic and the probability of acquisition of the lowest energy state becomes low resulting in increase of τ_{inc} with T . The optimal aggregation rate is reached at T_{min} (Fig. 6), where the entropy and energy factors reach a compromise.

The effect of template fixation is clearly seen in Fig. 6c for the (5+1)-system, where incorporation time onto FT, τ_{inc}^{FT} , is nearly one order of magnitude as high as the incorporation time onto NFT, τ_{inc}^{NFT} . The reason for the difference in incorporation times is the same as in the case of all-atom models, i.e. thermal fluctuations of NFT accommodate the added monomer.

The effect of template immobility for larger systems is shown in Fig. 7, where results were obtained at T_{min} . The influence on a template of three chains is minor, but for $N \geq 6$ fibril elongation on the fixed template slows down by one order of magnitude. Thus, within lattice models template fluctuations also speed up fibril growth. However, this result is more convincing than that based on all-atom models as it has been obtained for much larger system sizes.

If the number of chains in the template exceeds 11, both τ_{inc}^{FT} and τ_{inc}^{NFT} become scale invariant. Therefore we can consider $N_c = 11$ as the size of a critical nucleus at which the turn-over in system free energy occurs⁵¹. The same result has been obtained for other temperatures and fluctuating templates⁵¹. Thus, N_c seems to weakly depend on T , and template immobility does not have any effect on it.

IV. CONCLUSIONS

Using all-atom and lattice models, we have compared the kinetics of association of a nascent monomer with FT and NFT. It is shown that the immobility of the preformed template greatly hinders oligomer growth. Since fluctuations of the preformed template are expected to be small beyond the critical nucleus size, one can partially understand why fibril formation is a very slow process. Thus, together with other intrinsic and environmental properties, template flexibility is one of the important factors governing oligomerization rates.

Due to the existence of intermediates on some pathways toward the fibril state, kinetics can be described by the kinetic partitioning mechanism⁵⁶, where the fraction of trajectories without intermediates (Φ) reaches the ordered state rapidly, while the remaining fraction ($1 - \Phi$) gets kinetically trapped following different slow pathways. Consequently, the free energy landscape includes additional valleys representing intermediate states.

We speculate that our study demonstrates that a backbone entropy loss introduced through the fixation of C_α atoms opens up new kinetics routes with high energy barriers between intermediate and fibril states. Template rigidity deforms the FEL in such a way that a nascent peptide can explore newly available regions of energy landscape. Interestingly, instability of a mobile template has been pointed out as one of the factors governing oligomer growth³⁰. However, template rigidity does not eliminate the possibility of aggregation, but reduces the kinetics rate. This result proves that the flexibility of the preformed template has a significant impact on aggregation kinetics and is one of the general determinants of aggregation rates. Since template flexibility is very important, it would be interesting to check how a change of peptide flexibility caused by mutations might affect oligomerization kinetics. For example a Phe-Leu(Ile) mutation will enhance(decrease) peptide flexibility⁵⁷ while preserving hydrophobicity comparable to Phe. We are testing this idea of using the effects of amino acids substitution in the $A\beta_{16-22}$ sequence to fine-tune oligomerization rates in ongoing simulations.

ACKNOWLEDGMENTS

The work was supported by Department of Science and Technology at Ho Chi Minh city, National Foundation for Science and Technology Development (NAFOSTED) under grant number 106-YS.02-2013.01, Vietnam and Narodowe Centrum Nauki in Poland (grant No 2011/01/B/NZ1/01622) We would also like to acknowledge support from the TEAM project (TEAM/2011-7/6) cofinanced by the EU European Regional Development Fund operated within the Innovative Economy Operational Program and from Polish Ministry of Science and Higher Education Grant No. IP2012 016872. MSL thanks D. Eisenberg for correspondence.

* mkouza@chem.uw.edu.pl

† masli@ifpan.edu.pl

- ¹ Chiti F, Dobson CM (2006) Protein misfolding, functional amyloid, and human disease. *Annual Rev. Biochemistry* 75:333–366.
- ² Lomakin A, Chung DS, Bedenek GB, Kirschner DA, Teplow DB (1996) On the nucleation and growth of beta-protein fibrils: detection of nuclei and quantitation of rate constants. *Proc. Natl. Acad. Sci. USA* 93:1125–1129.
- ³ Rochet JC, Lansbury PT (2000) Amyloid fibrillogenesis: themes and variations. *Curr. Opin. Struct. Biol.* 10:60–68.
- ⁴ Wetzel R (2002) Ideas of order for amyloid fibril structure. *Structure* 10:1031–1036.
- ⁵ Selkoe DJ (2003) Folding proteins in fatal ways. *Nature* 426:900–904.
- ⁶ Dobson CM (2004) Protein chemistry. in the footsteps of alchemists. *Science* 304:1259–1262.
- ⁷ Ross CA, Poirier MA (2004) Protein aggregation and neurodegenerative disease. *Nature Med.* 10:S10–S17.
- ⁸ Bossy-Wetzel E, Schwarzenbacher R, Lipton SA (2004) Molecular pathways to neurodegeneration. *Nature Med.* 10:S2–S9.
- ⁹ Lee JC, Gray HB, Winkler JR (2005) Tertiary contact formation in alpha-synuclein probed by electron transfer. *J. Am. Chem. Soc.* 127:16388–16389.
- ¹⁰ Nelson R, Eisenberg D (2006) Structural models of amyloid-like fibrils. *Adv. Prot. Chem.* 73:235–282.
- ¹¹ Babenko V, Dzwolak W (2013) Amino acid sequence determinants in self-assembly of insulin chiral amyloid superstructures: Role of c-terminus of b-chain in association of fibrils. *FEBS Letters* 587:625–630.
- ¹² Gupta P, Hall CK, Voegler AC (1998) Effect of denaturant and protein concentrations upon protein refolding and aggregation: A simple lattice model. *Protein Sci.* 7:2642–2652.
- ¹³ Ma BY, Nussinov R (2002) Stabilities and conformations of alzheimer’s beta-amyloid peptide oligomers (a beta(16-22 ’) a beta(16-35 ’) and a beta(10-35)): Sequence effects. *Proc. Natl. Acad. Sci. USA* 99:14126–14131.
- ¹⁴ Massi F, Straub JE (2001) Energy landscape theory for alzheimer’s beta-peptide fibril elonga-

- tion. *Proteins* 42:217–229.
- 15 Smith AV, Hall CK (2001) Protein refolding versus aggregation: Computer simulations on an intermediate-resolution protein model. *J. Mol. Biol.* 312:187–202.
 - 16 Gsponer J, Haberthur U, Caflisch A (2003) The role of side-chain interactions in the early steps of aggregation: Molecular dynamics simulations of an amyloid-forming peptide from the yeast prion sup351. *Proc. Natl. Acad. Sci. USA* 100:5154–5159.
 - 17 Klimov DK, Thirumalai D (2003) Dissecting the assembly of A beta(16-22) amyloid peptides into antiparallel beta sheets. *Structure* 11:295–307.
 - 18 Favrin G, Irback A, Mohanty S (2004) Oligomerization of amyloid a β (16-22) peptides using hydrogen bonds and hydrophobicity forces. *Biophys. J* 87:3657–3664.
 - 19 Wei GH, Mousseau N, Derreumaux P (2004) Sampling the self-assembly pathways of kffe hexamers. *Biophys. J.* 87:3648–3656.
 - 20 Buchete NV, Tycko R, Hummer G (2005) Molecular dynamics simulations of alzheimer’s beta-amyloid protofilaments. *J. Mol. Biol.* 353:804–821.
 - 21 Malolepsza E, Boniecki M, Kolinski A, Piela L (2005) Theoretical model of prions: a misfolded protein induces misfolding. *Proc. Natl. Acad. Sci. (USA)* 102:7835–7840.
 - 22 Conchillo-Sole O, et al. (2007) Aggrescan: a server for the prediction and evaluation of hot spots of aggregation in polypeptides. *BMC BIOINFORMATICS* 8:65.
 - 23 Takeda T, Klimov DK (2007) Dissociation of a beta(16-22) amyloid fibrils probed by molecular dynamics. *J. Mol. Biol* 368:1202–1213.
 - 24 Bellesia G, Shea JE (2007) Self-assembly of beta-sheet forming peptides into chiral fibrillar aggregates. *J. Chem. Phys.* 126:245104.
 - 25 Baumketner A, Shea JE (2007) The structure of the alzheimer amyloid beta 10-35 peptide probed through replica-exchange molecular dynamics simulations in explicit solvent. *J. Mol. Biol* 366:275–285.
 - 26 Li MS, Co NT, Hu CK, Straub JE, Thirumalai D (2010) Determination of factors governing fibrillogenesis of polypeptide chains using lattice models. *Phys. Rev. Lett* 105:218101.
 - 27 Rojas AV, Liwo A, Scheraga HA (2011) A study of the α -helical intermediate preceding the aggregation of the amino-terminal fragment of the amyloid peptide (A(1-28)). *J Phys Chem B* 115:12978–12983.
 - 28 Esler WP, et al. (2000) Alzheimer’s disease amyloid propagation by a template-dependent

- dock-lock mechanism. *Biochemistry* 39:6288–6295.
- ²⁹ Cannon MJ, Williams AD, Wetzel R, Myszka DG (2004) Kinetic analysis of beta-amyloid fibril elongation. *Anal. Biochem.* 328:67–75.
- ³⁰ Nguyen PH, Li MS, Stock G, Straub JE, Thirumalai D (2007) Monomer adds to preformed structured oligomers of $\alpha\beta$ -peptides by a two-stage dock-lock mechanism. *Proc. Natl. Acad. Sci. (USA)* 104:111–116.
- ³¹ Reddy R, Straub JE, Thirumalai D (2009) Dynamics of locking of peptides onto growing amyloid fibrils. *Proc. Natl. Acad. Sci. (USA)* 106:11948–11953.
- ³² Jarrett JT, Lansbury PT (1993) Seeding one-dimensional crystallization of amyloid: A pathogenic mechanism in alzheimer’s disease and scrapie? *Cell* 73:1055–1058.
- ³³ Serio TR, et al. (2000) Nucleated conformational conversion and the replication of conformational information by a prion determinant. *Science* 289:1317–1321.
- ³⁴ Collins SR, Douglass A, Vale RD, Weissman JS (2004) Mechanism of prion propagation: Amyloid growth occurs by monomer addition. *PLOS Biol.* 2:1582–1590.
- ³⁵ Rojas A, Liwo A, Browne D, Scheraga HA (2010) Mechanism of fiber assembly: Treatment of a peptide aggregation with a coarse-grained united-residue force field. *Journal of Molecular Biology* 404:537 – 552.
- ³⁶ van Gunsteren W, et al. (1996) *Biomolecular Simulation: The GROMOS96 Manual and User Guide*. (Vdf Hochschulverlag AG an der ETH, Zurich).
- ³⁷ Li MS, Klimov DK, Straub JE, Thirumalai D (2008) Probing the mechanisms of fibril formation using lattice models. *J. Chem. Phys.* 129:175101.
- ³⁸ Berendsen HJC, Postma J, van Gunsteren W, Hermans J (1996) *Intermolecular Forces* (Reidel, Dordrecht).
- ³⁹ Wabik J, Kmiecik S, Gront D, Kouza M, Kolinski A (2013) Combining coarse-grained protein models with replica-exchange all-atom molecular dynamics. *Int. J. Mol. Sc.* 14:9893–9905.
- ⁴⁰ Kouza M, Hu CK, Zung H, Li M (2009) Protein mechanical unfolding: Importance of non-native conformations. *J. Chem. Phys.* 131:215103.
- ⁴¹ Nam HB, Kouza M, Zung H, Li MS (2010) Relationship between population of the fibril-prone conformation in the monomeric state and oligomer formation times of peptides: Insights from all-atom simulations. *J. Chem. Phys.* 132:165104.
- ⁴² Nguyen PH, Li MS, Derreumaux P (2011) Effects of all-atom force fields on amyloid oligomer-

- ization: replica exchange molecular dynamics simulations of the a beta(16-22) dimer and trimer. *Phys. Chem. Chem. Phys.* 13:9778–9788.
- ⁴³ Lee JP, et al. (1995) ¹hnmr of a β amyloid peptide congeners in water solution. conformational changes correlate with plaque competence. *Biochem.* 34:5191–5200.
- ⁴⁴ Mu Y, Nguyen P, Stock G (2005) Energy landscape of a small peptide revealed by dihedral angle principle component analysis. *Proteins* 58:45–52.
- ⁴⁵ Cecchini M, Rao F, Seeber M, Caffisch A (2004) Replica exchange molecular dynamics simulations of amyloid peptide aggregation. *J. Chem. Phys.* 121:10748–10756.
- ⁴⁶ Kolinski A (2004) Protein modeling and structure prediction with a reduced representation. *Acta Biochimica Polonica* 51:349–371.
- ⁴⁷ Kmiecik S, Gront D, Kouza M, Kolinski A (2012) From coarse-grained to atomic-level characterization of protein dynamics: transition state for the folding of b domain of protein a. *J. Phys. Chem. B* 116:7026–7032.
- ⁴⁸ Jamroz M, Orozco M, Kolinski A, Kmiecik S (2013) Consistent view of protein fluctuations from all-atom molecular dynamics and coarse-grained dynamics with knowledge-based force-field. *J. Chem. Theory Comput.* 9(1):119–125.
- ⁴⁹ Hilhorst HJ, Deutch JM (1975) Analysis of monte-carlo results on kinetics of lattice polymer-chains with excluded volume. *J. Chem. Phys.* 63:5153–5161.
- ⁵⁰ Li MS, Klimov DK, Thirumalai D (2002) Dependence of folding rates on protein length. *J. Phys. Chem. B* 106:8302–8305.
- ⁵¹ Co NT, Li MS (2012) New method for determining size of critical nucleus of fibril formation of polypeptide chains. *J. Chem. Phys.* 137:095101.
- ⁵² Co NT, Hu CK, Li MS (2013) Dual effect of crowders on fibrillation kinetics of polypeptide chains revealed by lattice models. *J Chem Phys* 138:185101.
- ⁵³ Colletier JP, et al. (2011) Molecular basis for amyloid-beta polymorphism. *Proc. Natl. Acad. Sci. U.S.A.* 108:16938–16943.
- ⁵⁴ Cieplak M, Hoang TX, Li MS (1999) Scaling of folding properties in simple models of proteins. *Phys. Rev. Lett.* 83:1684–1687.
- ⁵⁵ Li MS, Cieplak M (1999) Folding in two-dimensional off-lattice models of proteins. *Phys. Rev. E* 59:970–976.
- ⁵⁶ Thirumalai D, Klimov DK, Woodson SA (1997) Kinetic partitioning mechanism as a unifying

theme in the folding of biomolecules. *Theor. Chem. Accounts* 96:14–22.

⁵⁷ Huang F, Nau WM (2003) A conformational flexibility scale for amino acids in peptides. *Angew. Chem. Int. Ed.* 42:2269–2272.

⁵⁸ See supplementary material at xxx for the structure and fibril formation times of the double layer system, and figures on time dependence of order parameter P_2 and HBs of double layer (8+1) and single layer (4+1) systems.

Table

TABLE I. $\bar{\tau}_{\text{inc}}$ of individual trajectories of all-atom MD runs for three systems with FT. The whole simulation time is shown in parentheses.

| System | Time (ns) | | |
|--------|-------------|-------------|-------------|
| | 3+1 | 4+1 | 5+1 |
| Tr1 | 19.4 (178) | > 500(500) | 179.5 (500) |
| Tr2 | 383.5 (500) | 138 (500) | 321 (500) |
| Tr3 | > 500(500) | 247.5 (500) | > 500(500) |
| Tr4 | > 500(500) | 486.5 (500) | 212 (500) |
| Tr5 | 411.7 (500) | > 500(500) | > 500(500) |
| Tr6 | 102.3 (200) | > 500(500) | > 500(500) |
| Tr7 | 43.7 (200) | 31.5 (200) | > 500(500) |
| Tr8 | 13.5 (200) | 426.5 (500) | > 500(500) |
| Tr9 | | 96.4 (500) | |
| Tr10 | | > 500(500) | |
| Tr11 | | 345.2 (500) | |
| Tr12 | | 165.9 (500) | |
| Tr13 | | > 500(500) | |
| Tr14 | | 498.5 (500) | |
| Tr15 | | > 500(500) | |
| Tr16 | | > 500(500) | |

TABLE II. $\bar{\tau}_{\text{inc}}$ obtained for FT and NFT cases. The results were averaged over 4 trajectories for NFT. The median time, i.e. the mean of the 4th and 5th values from 8 trajectories, is used for FT.

| System | not fixed template | fixed template |
|--------|--------------------|----------------|
| 3 + 1 | 23 | 242.9 |
| 4 + 1 | 114 | 456.5 |
| 5 + 1 | > 220 | > 500 |

Figure Captions

Fig. 1:: The templates used in our simulations, where (a), (b), and (c) are for the (3+1)-, (4+1) and (5+1)-system, respectively. These configurations were obtained by long MD simulations with the Gromos 43a1 force field in our prior work³⁰. P_i refers to peptide i .

Fig. 2:: The time dependence of order parameter P_2 (right scale) and number of backbone HBs between nascent peptide and FT (left scale) for four trajectories of the (3+1)-system. Black curve corresponds to P_2 , while the curves representing number of HBs between nascent peptide and one of peptides from FT are colored according to the legend on Fig. 2 for Tr1. Here AP- P_i refers to backbone HBs between added peptide and peptide i that belongs to the template. The nascent peptide $A\beta_{16-22}$ shown on snapshots is colored in green. The fibril antiparallel arrangement occurs in all trajectories except the Traj3 and Traj4.

Fig. 3:: The same as in Fig. 2 but for the (4+1)-system. Black curve corresponds to P_2 , while the curves representing number of HBs between nascent peptide and one of peptides from FT are colored according to the legend on Fig. 3 for Tr5. The fibril antiparallel arrangement occurs in the trajectories 2-4, 7 and 8, but not in the first, fifth and sixth ones. Unexpected parallel ordering is observed in the first run, where the nascent peptide is docked by the edge of the template.

Fig. 4:: The same as in Fig. 2 but for the (5+1)-system. Black curve corresponds to P_2 , while the curves representing number of HBs between nascent peptide and one of peptides from FT are colored according to the legend on Fig. 4 for Tr1. The fibril arrangement occurs in the first and second trajectories but not in the third and fourth one ones. In the second trajectory the parallel orientation of the added peptide occurs (at $t \approx 62$ ns) earlier than the antiparallel one (at $t \approx 321$ ns).

Fig. 5:: Free energy surface of trajectory 8 (a) and trajectory 3 (b) for the (3+1) systems and of trajectory 2 (c) and trajectory 3 (d) for the (5+1) systems. **The first and second eigenvectors of the fluctuations covariance matrix used for construction of FEL's account for roughly 62 % of the whole information about the systems studied.**

In trajectory 1 of (3+1) system and trajectory 2 of (5+1) system the fast association of the nascent with the fixed template is observed. For trajectory 3 of both systems the fibril state does not occur after 500 ns.

Fig. 6:: A typical initial conformation for the (5+1) system in the lattice model. Five template monomers are antiparallel, while the conformation of a nascent monomer is randomly generated. (b) The fibril conformation with the lowest energy $E = -60$. (c) The temperature dependence of τ_{inc} for NFT and FT cases. $T_F = 0.5\epsilon_H/k_B$ is the folding temperature for the monomer. The results are averaged over 50 MC trajectories.

Fig. 7:: Dependence of τ_{inc} on the number of chains of FT and NFT in the lattice model. The values of τ_{inc} are collected at $T = T_{\text{min}}$ (see Fig. 6). The arrow refers to the size of critical nucleus $N_c = 11$ where τ_{inc} starts to saturate. For each value of N the results are averaged over 50 MC runs.

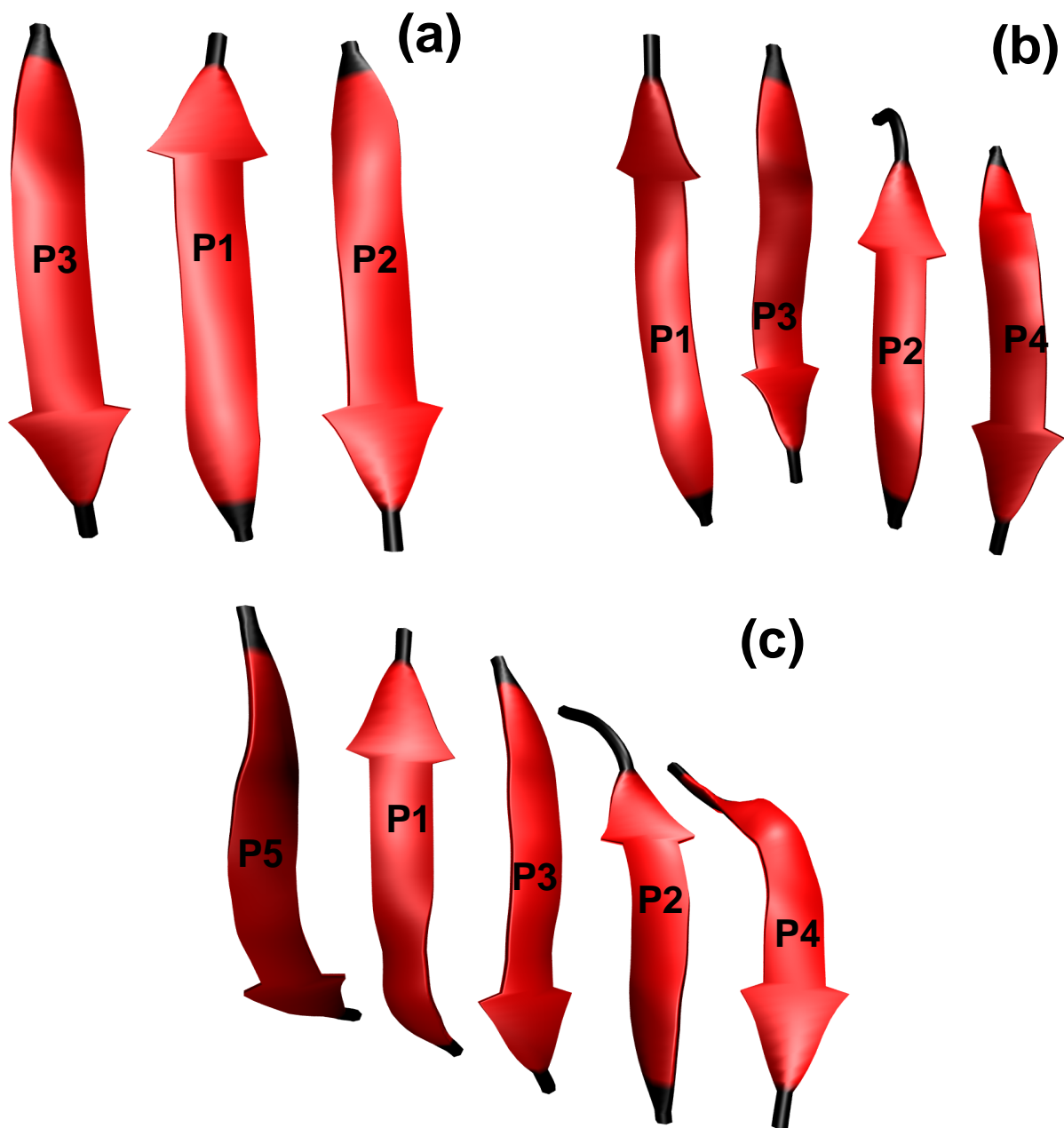


FIG. 1. The templates used in our simulations, where (a), (b), and (c) are for the (3+1)-, (4+1) and (5+1)-system, respectively. These configurations were obtained by long MD simulations with the Gromos 43a1 force field in our prior work³⁰. P_i refers to peptide i .

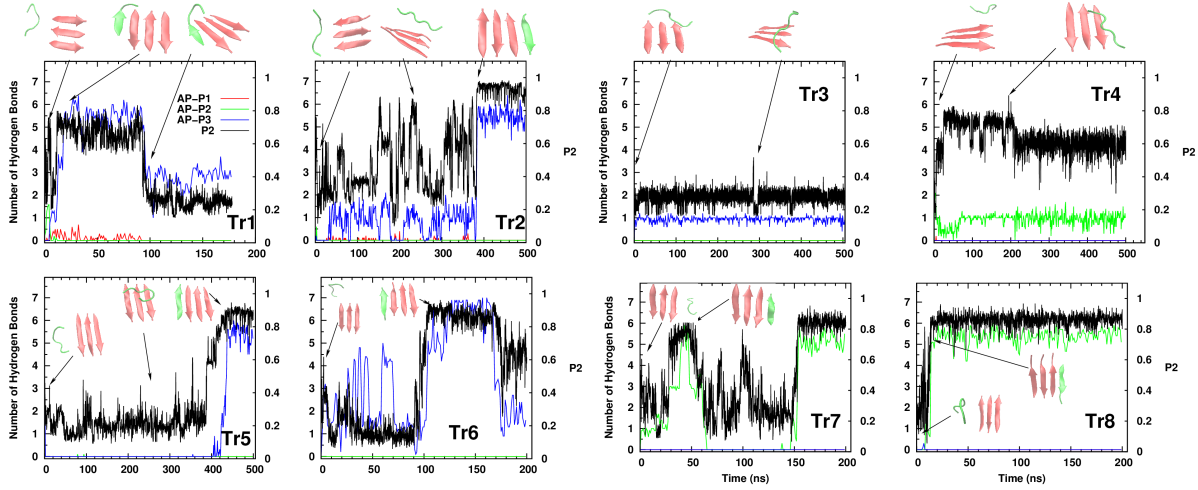


FIG. 2. The time dependence of order parameter P_2 (right scale) and number of backbone HBs between nascent peptide and FT (left scale) for four trajectories of the (3+1)-system. Black curve corresponds to P_2 , while the curves representing number of HBs between nascent peptide and one of peptides from FT are colored according to the legend on Fig. 2 for Tr1. Here AP- P_i refers to backbone HBs between added peptide and peptide i that belongs to the template. The nascent peptide $A\beta_{16-22}$ shown on snapshots is colored in green. The fibril antiparallel arrangement occurs in all trajectories except the Traj3 and Traj4.

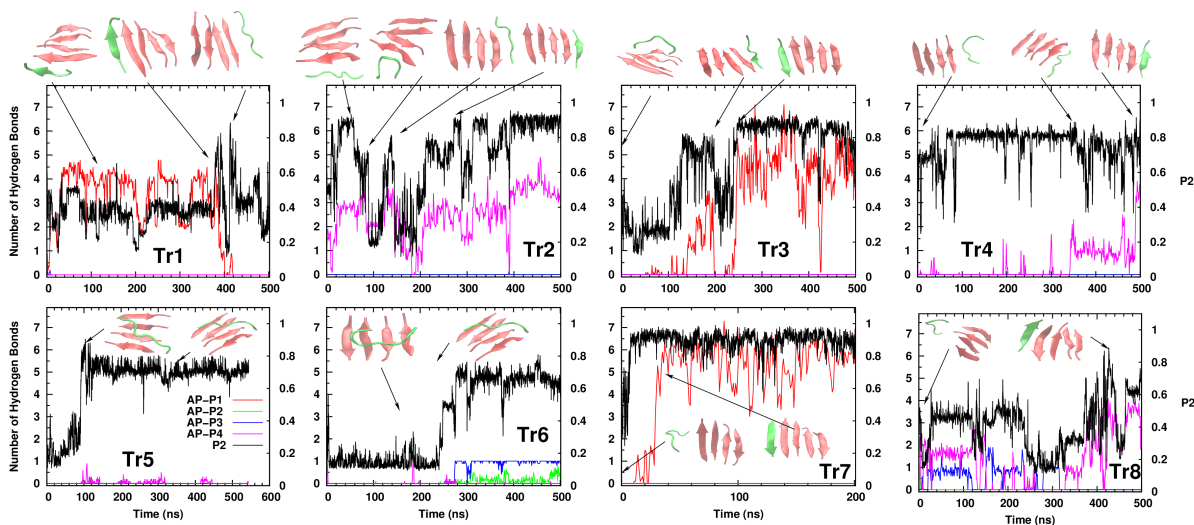


FIG. 3. The same as in Fig. 2 but for the (4+1)-system. Black curve corresponds to P_2 , while the curves representing number of HBs between nascent peptide and one of peptides from FT are colored according to the legend on Fig. 3 for Tr5. The fibril antiparallel arrangement occurs in the trajectories 2-4, 7 and 8. but not in the first, fifth and sixth ones. Unexpected parallel ordering is observed in the first run, where the nascent peptide is docked by the edge of the template.

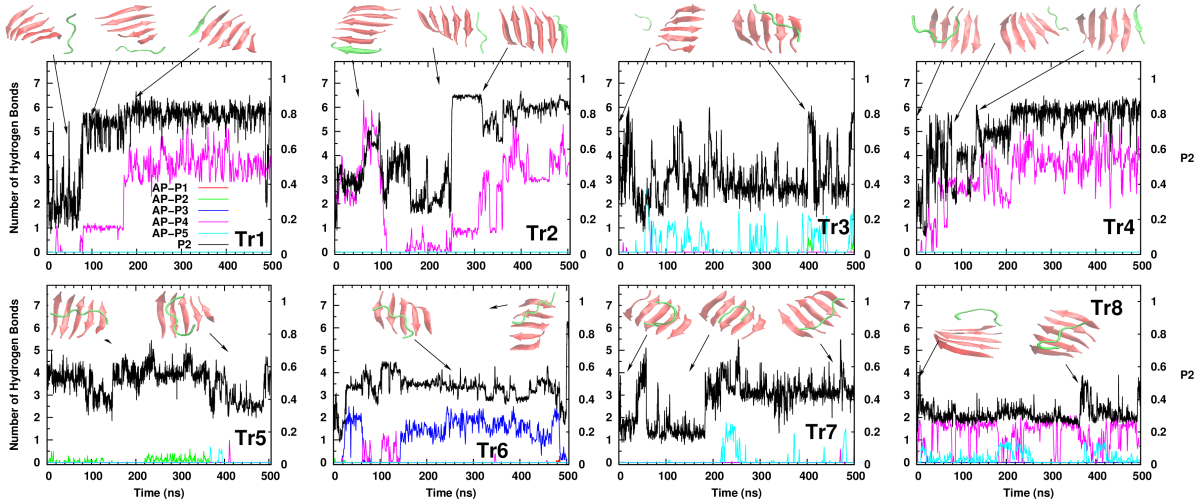


FIG. 4. The same as in Fig. 2 but for the (5+1)-system. Black curve corresponds to P_2 , while the curves representing number of HBs between nascent peptide and one of peptides from FT are colored according to the legend on Fig. 4 for Tr1. The fibril arrangement occurs in the first and second trajectories but not in the third and fourth one ones. In the second trajectory the parallel orientation of the added peptide occurs (at $t \approx 62$ ns) earlier than the antiparallel one (at $t \approx 321$ ns).

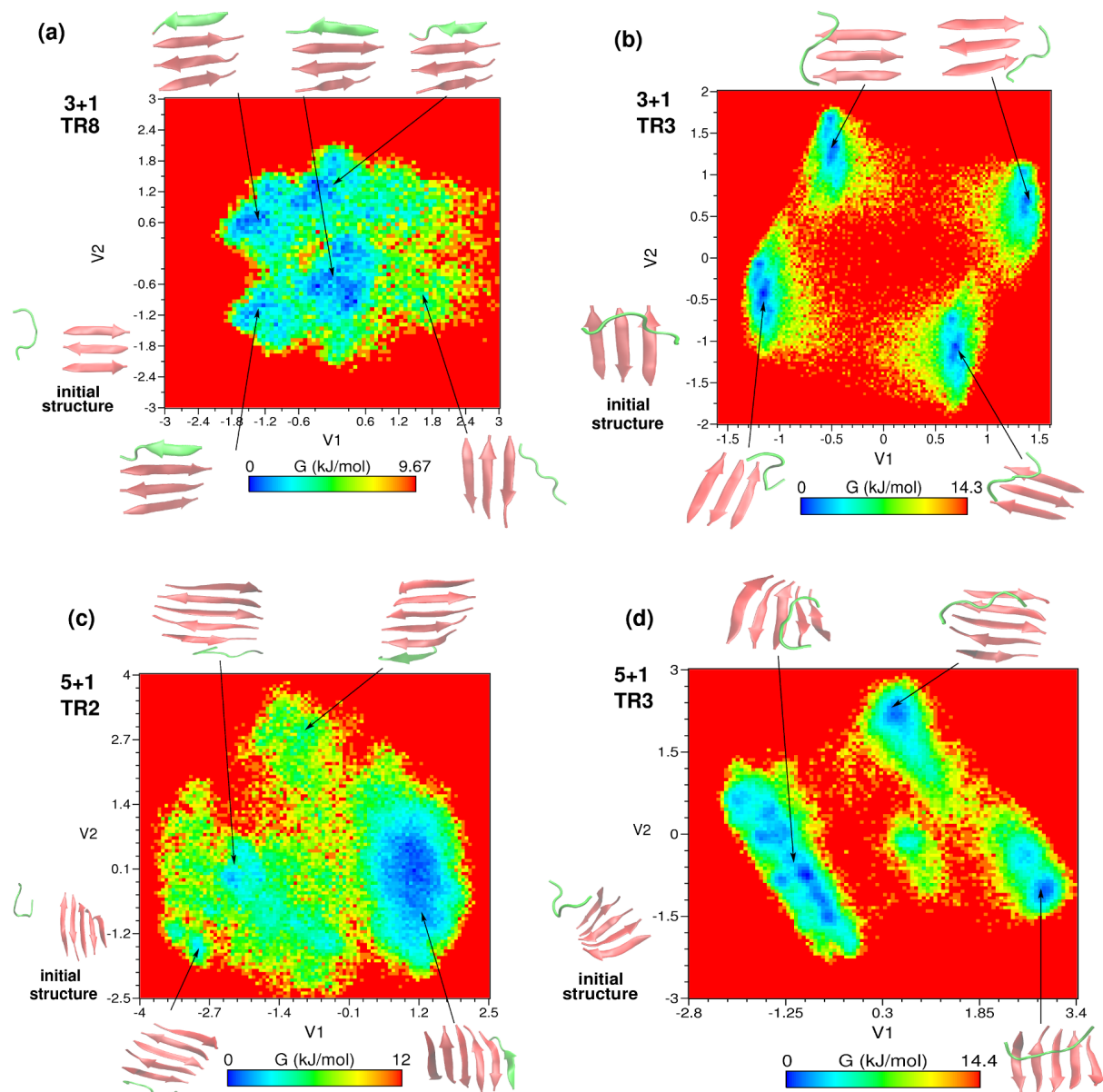


FIG. 5. Free energy surface of trajectory 8 (a) and trajectory 3 (b) for the (3+1) systems and of trajectory 2 (c) and trajectory 3 (d) for the (5+1) systems. The first and second eigenvectors of the fluctuations covariance matrix used for construction of FEL's account for roughly 62 % of the whole information about the systems studied. In trajectory 1 of (3+1) system and trajectory 2 of (5+1) system the fast association of the nascent with the fixed template is observed. For trajectory 3 of both systems the fibril state does not occur after 500 ns.

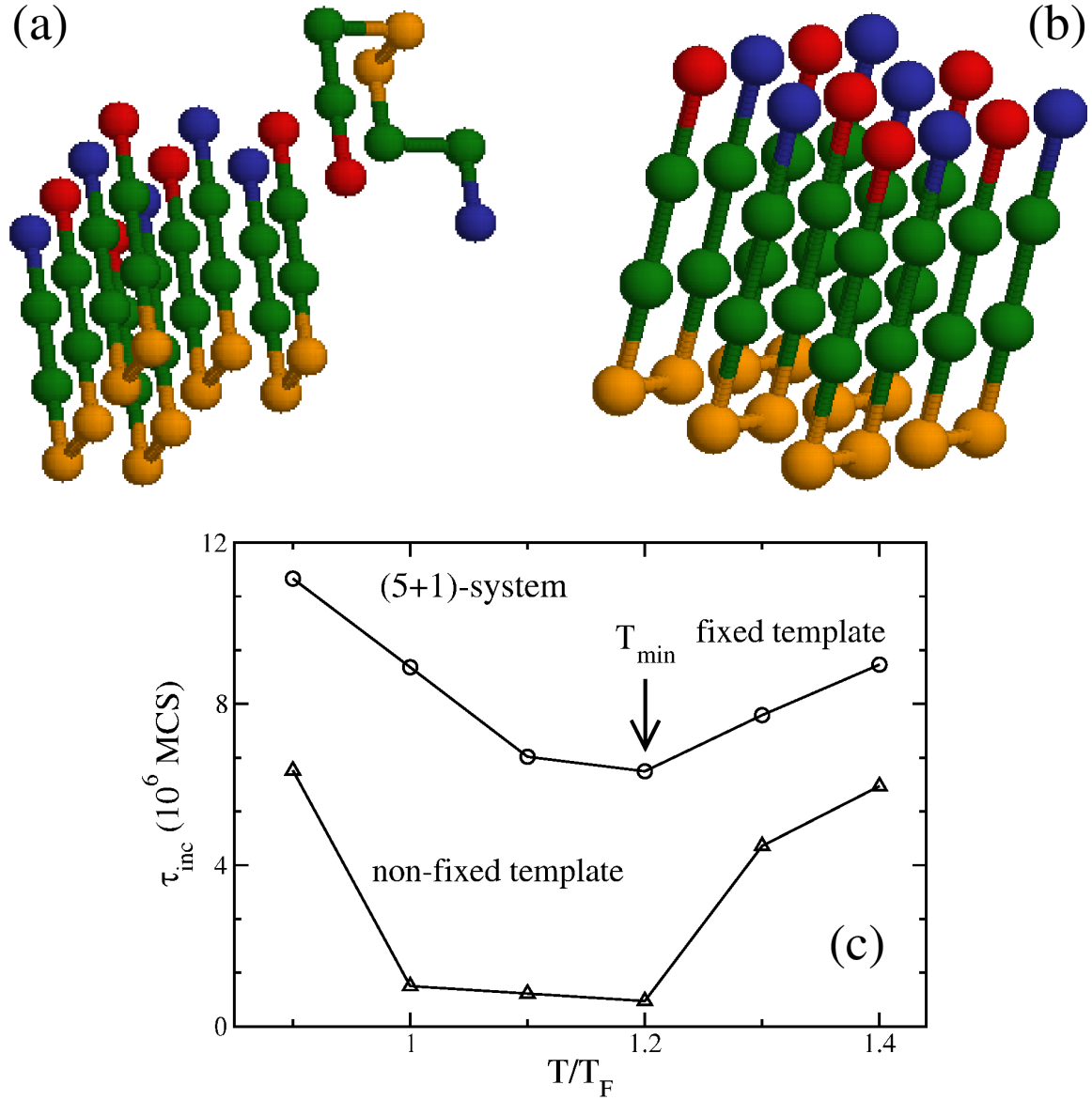


FIG. 6. (a) A typical initial conformation for the (5+1) system in the lattice model. Five template monomers are antiparallel, while the conformation of a nascent monomer is randomly generated. (b) The fibril conformation with the lowest energy $E = -60$. (c) The temperature dependence of τ_{inc} for NFT and FT cases. $T_F = 0.5\epsilon_H/k_B$ is the folding temperature for the monomer. The results are averaged over 50 MC trajectories.

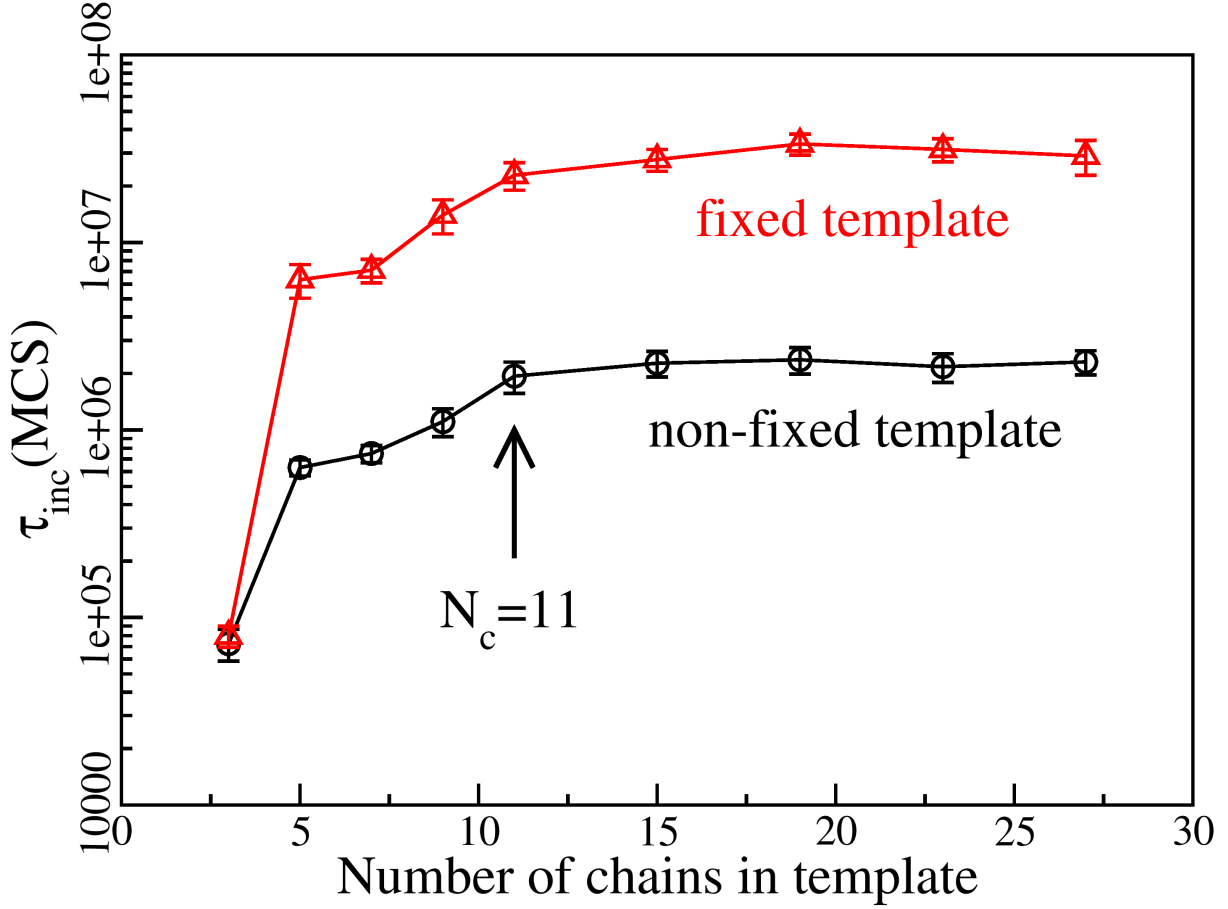


FIG. 7. Dependence of τ_{inc} on the number of chains of FT and NFT in the lattice model. The values of τ_{inc} are collected at $T = T_{\text{min}}$ (see Fig. 6). The arrow refers to the size of critical nucleus $N_c = 11$ where τ_{inc} starts to saturate. For each value of N the results are averaged over 50 MC runs.

Supporting information for:

**Preformed template fluctuations promote fibril
formation: Insights from lattice and all-atom models**

Maksim Kouza,^{*,†} Nguyen Truong Co,[‡] Phuong H. Nguyen,[¶] Andrzej Kolinski,[†]
and Mai Suan Li^{*,§}

*Faculty of Chemistry University of Warsaw, ul. Pasteura 1, 02-093 Warszawa Poland, Institute for
Computational Science and Technology, 6 Quarter, Linh Trung Ward, Thu Duc District, Ho Chi
Minh City, Vietnam, Laboratoire de Biochimie Theorique, UPR 9080 CNRS, IBPC, Universite
Paris 7, 13 rue Pierre et Marie Curie, 75005, Paris, France, and Institute of Physics, Polish
Academy of Sciences, Al. Lotnikow 32/46, 02-668 Warsaw, Poland*

E-mail: mkouza@chem.uw.edu.pl; masli@ifpan.edu.pl

Supplementary Information

*To whom correspondence should be addressed

[†]Faculty of Chemistry University of Warsaw

[‡]Institute for Computational Science and Technology

[¶]Universite Paris 7

[§]Institute of Physics Polish, Academy of Sciences

Table S1: $\bar{\tau}_{\text{inc}}$ of individual trajectories of all-atom MD runs for double layer (8+1)-systems with NFT and FT. The whole simulation time is shown in parentheses.

| System | Time (ns) | |
|--------|-------------|------------|
| | 8+1 (NFT) | 8+1 (FT) |
| Tr1 | 43.7 (200) | > 400(400) |
| Tr2 | 1.2 (200) | > 400(400) |
| Tr3 | 159.8 (200) | > 400(400) |
| Tr4 | 129.1 (200) | 200.3(400) |

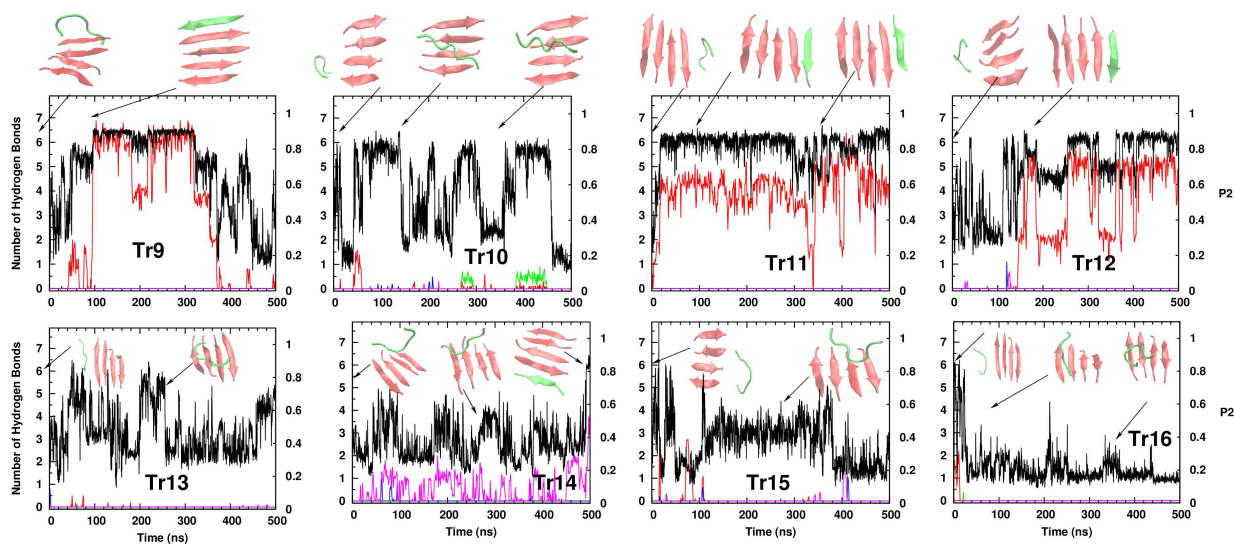


Figure S1: The time dependence of order parameter P_2 (right scale) and number of backbone HBs between nascent peptide and FT(left scale) for Trajs 9 to 16 of the 4+1 system. Black curve corresponds to P_2 , while the curves representing number of HBs between nascent peptide and one of peptides from FT are colored according to the legend on Fig. 3, Tr5. Here AP- P_i refers to backbone HBs between added peptide and peptide i that belongs to the template. The nascent peptide $A\beta_{16-22}$ shown on snapshots is colored in green.

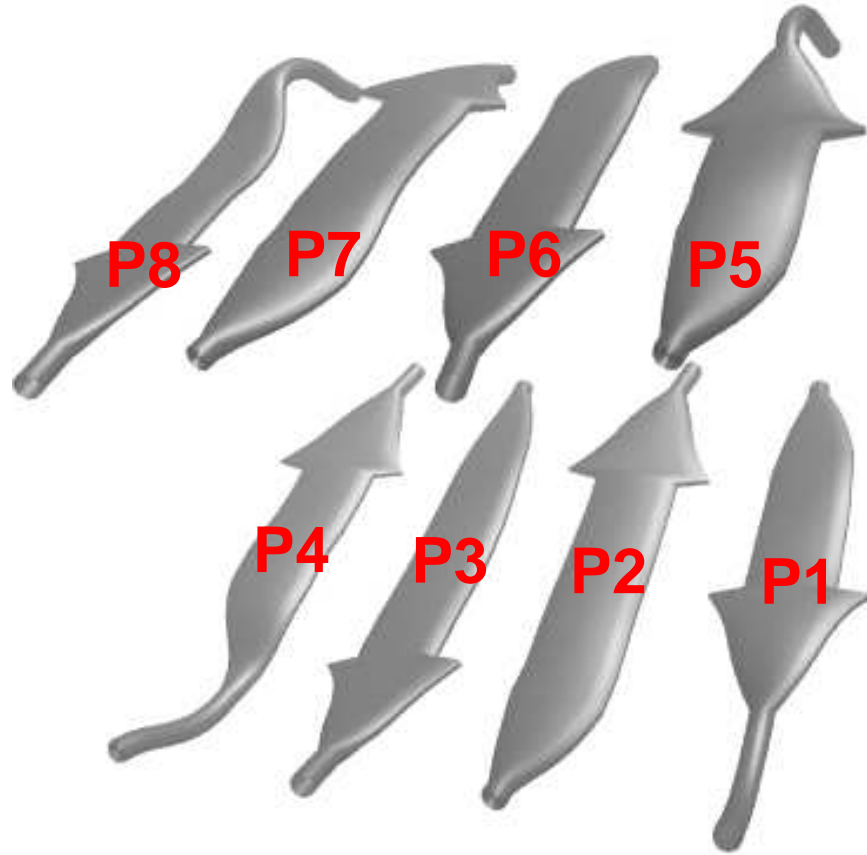


Figure S2: The template of double layer KLVFFA oligomer used in FT and NFT simulations. This template configuration was obtained from available experimentally structure^{S1} (pdb code: 3OW9). P_i refers to peptide i .

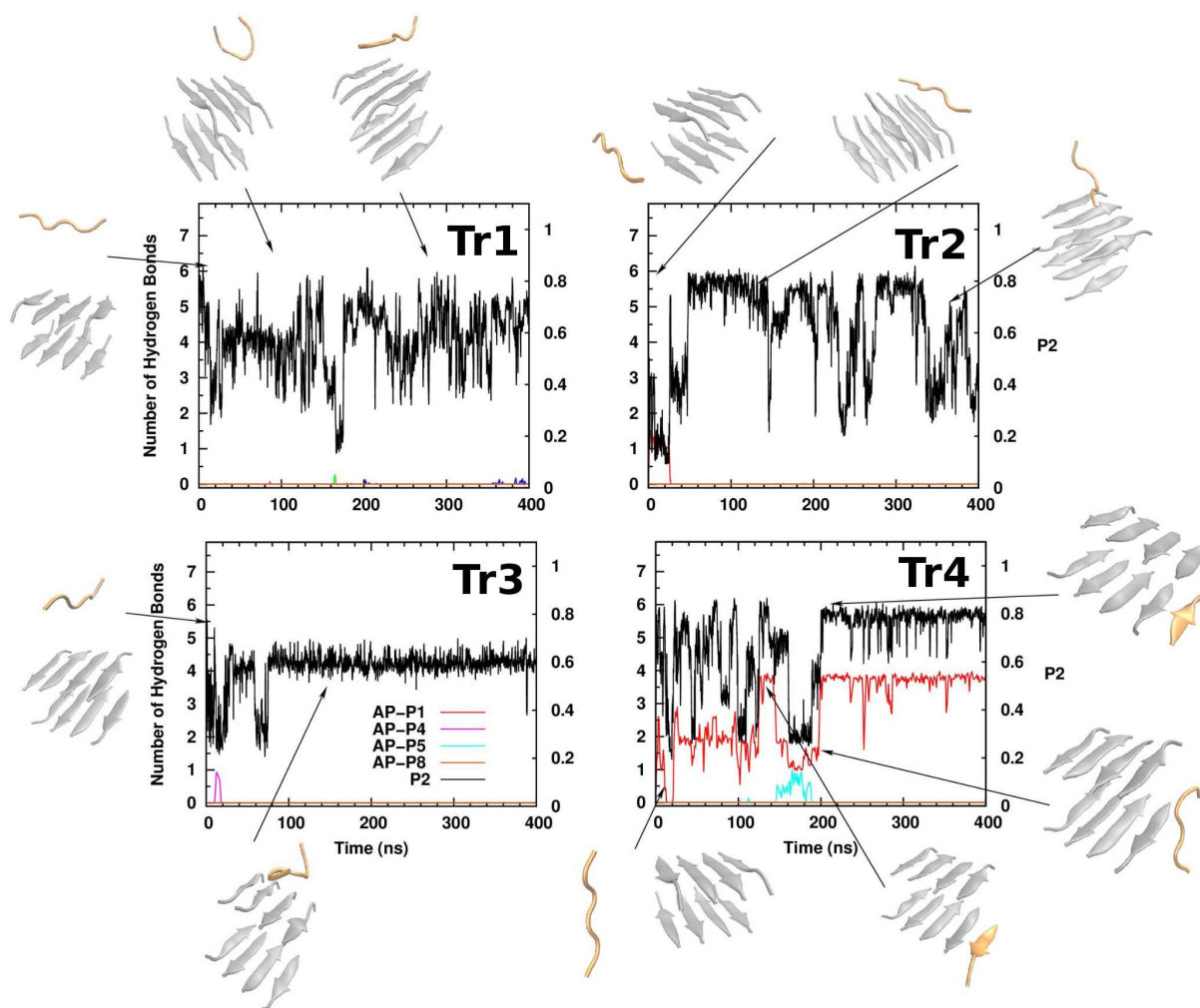


Figure S3: The time dependence of order parameter P_2 (right scale) and number of backbone HBs between nascent peptide and FT(left scale) for Trajectory 1, 2, 3, and 4 for the double layer KLVFFA (8+1)-system with FT. Black curve corresponds to P_2 , while the curves representing number of HBs between nascent peptide and one of peptides from template are colored according to the legend on Fig. S3c. Here AP- P_i refers to backbone HBs between added peptide and peptide i that belongs to the template. The nascent peptide $A\beta_{16-22}$ shown on snapshots is colored in orange and the template is shown in silver. The fibril antiparallel arrangement occurs in Tr4, but not in Tr1, Tr2 and Tr3.

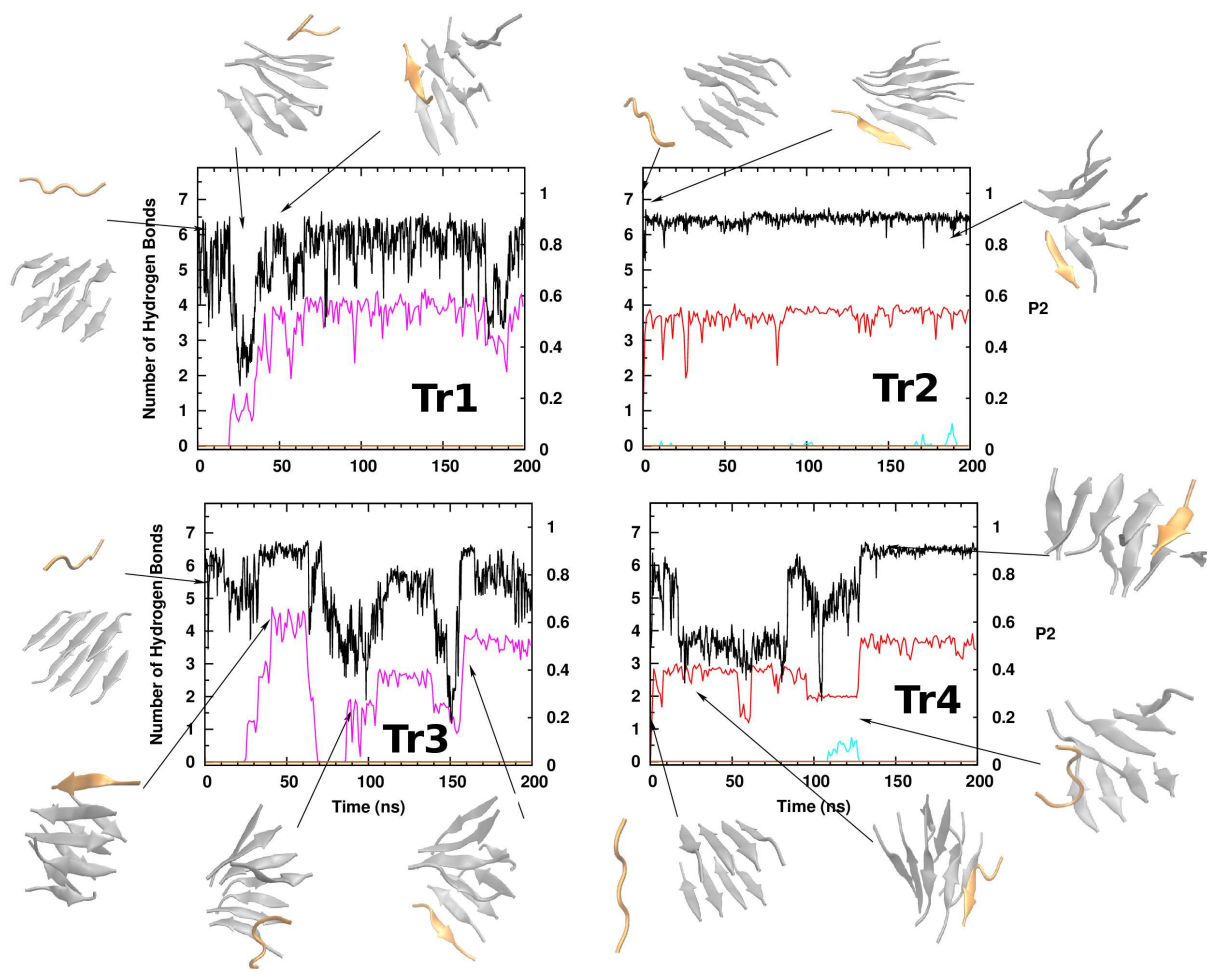


Figure S4: The same as in Fig. S3 but the for the double layer KLVFFA (8+1)-system with NFT. The fibril antiparallel arrangement occurs in all 4 trajectories, at 47.3, 1.2, 159.8 and 129.1 ns for Tr1, Tr2, Tr3 and Tr4, respectively. Parallel ordering is observed in the third run at 42 ns

References

- (S1) Colletier JP, et al. (2011) Molecular basis for amyloid-beta polymorphism. *Proc. Natl. Acad. Sci. U.S.A.* 108:16938–16943.